Identification of goaf instability under blasting disturbance using microseismic monitoring technology

Hanwen Jia · Baoxu Yan · Zhen Yang · Erol Yilmaz

Abstract Micro-seismic (MS) technique can be used to appreciate rock failure process and severity of damage by quantifying micro-earthquakes in terms of time, location, grade, and energy release. Based on 3D laser detection and high-precision micro-seismic monitoring, this study analyzes the MS activity, stress and displacement evolution linked with the instability/failure property of hidden goaf incorporating several blasting disturbances in an open pit mine. MS monitoring outcomes reveal two arch fracture zones in the goaf roof, and MS occasions are mostly intense at rock-intersecting interface of north–south goafs. Evolution of apparent stress, apparent volume, and displacement reveals that the goaf is currently in a stable state. The current investigation offers a novel field method and view of inspecting the stability of goaf subjected to blasting disturbance in mines.

Article Highlights

(1) With the blasting disturbance of the upper platform, two arched fracture zones formed on the roof of the goaf.
(2) Inversion of seismic source parameters indicates that the boundary between the north and south airspace is a danger prone area.
(3) The roof of the goaf near the foot of the slope is a potential area of collapse and damage.

H. Jia (✉)
Shandong Gold Group Co., Ltd., Jinan 250000, China
e-mail: jiahanwen@sd-gold.com

H. Jia
Center for Rock Instability and Seismicity Research, School of Resource and Civil Engineering, Northeastern University, Shenyang 110819, China

B. Yan
Key Laboratory of Western Mine Exploitation and Hazard Prevention, Ministry of Education, Energy School, Xi'an University of Science and Technology, Xi'an 710054, China

Z. Yang
Shandong Huanghe Ecological Development Group Co., Ltd., Jinan 250000, China

E. Yilmaz
Department of Civil Engineering, Geotechnical Division, Recep Tayyip Erdogan University, 53100 Fener, Rize, Turkey

1 Introduction

Goaf refers to mined-out areas after the mining of ore in underground mines (Jia et al. 2021). In the early stages of underground mining, metal mines usually use mining methods such as open-stope method and short-hole shrinkage method, resulting in the creation

of many goafs and their widespread distribution underground (Yan et al. 2022; Yin et al. 2020). The existence of goafs creates a severe risk to the security of mines, easily giving rise to various mine disasters and accidents (e.g., roof caving, collapsing, rib failure, and flooding (Juang et al. 2022; Tian et al. 2021; Zhang et al. 2023; Zhuang et al. 2022). The collapsed rocks in the goaf will suddenly compress the air and generate shock waves, which may govern fatalities and harms to tools and structures (Huo et al. 2022; Xie et al. 2022b; Zou et al. 2021). Goaf collapse may also damage the impermeable layer and cause underground water inrush (Liu et al. 2022).

Shallow goaf's large-scale collapse can cause surface collapse, leading to damage to surface buildings and casualties, and even triggering mining earthquakes, mountain landslides (Zhang et al. 2019). Historically left goaf is often not addressed in a timely manner due to reasons such as missing design data. Thus, lie concealed goaf's stability is important for a fruitful surface mining process due to its uncertainty of position, size and shape caused by people's illegal mining of ores (Emmanuel et al. 2018). Goaf collapses could be induced by multiple blasting or other dynamic disturbance during mine production process (Wang et al. 2013; Zhao et al. 2020; Zhou et al. 2018; Zhu et al. 2022).

Investigation of stability analysis and evaluation methods for goaf has always been a hot topic of concern (Jia et al. 2022; Kaya and Tarakçi 2021; Mánica et al. 2020; Talibe Keita et al. 2021; Xia et al. 2019). Its influencing factors mainly include hydrogeological and natural circumstances (e.g., the burial distance, inclination position, width, and lithology of ore body layers, as well as human aspects (e.g., mining methods, blasting disturbances, and mining frequency) (Ram et al. 2022; Saeidi et al. 2021; Wang et al. 2023). The research methods mainly cover theoretic/physical work, arithmetic model, and on-site monitoring methods (Karian et al. 2016; Seymour et al. 2019; Xu et al. 2015; Yan et al. 2023). To reduce the risk of roof fall, water inrush, and surface collapse caused by the instability and failure of goaf, the in-situ monitoring methods have become a research hotspot in mine disaster prevention and control (Xu et al. 2021). Goaf's stability observing largely adopts the method of either point or field observing. The first chiefly covers interior stress observing, surface movement watching, and inner dislocation observing of rock

mass. The latter mostly covers micro-seismic (MS) observing and electromagnetic radiation observing, among which MS monitoring is considered a very effective field monitoring method for evaluating the stability of goaf (Dyskin et al. 2018; Wang et al. 2021).

MS technology, aka micro earthquake, refers to vibration generated by the internal crack growth of rocks under external action (Chen et al. 2022; Ma et al. 2022; Zhao et al. 2021b), which propagates in the form of waves (Dong et al. 2015). This phenomenon is more obvious for the rock in an anisotropic stress state and influenced by the geological structures and engineering disturbances (Chen et al. 2023; Xie et al. 2022a). To further record and analyze the regularity of this vibration wave, several micro-seismic parameters in terms of time, location, grade and energy release are determined (Huang et al. 2018), and finally determine the stability of rock mass within the monitoring range, a complete monitoring technology, namely MS monitoring technology, has been gradually formed (Ge 2005; Tang et al. 2010). Maxwell et al. (Maxwell et al. 2010) employed the micro-seismic information to detect seismic events of creation of a oil basin that escort injections into or manufacture from basin. Liu et al. (2017) studied comprehensively the critical aspects of road instability over the whole failure growth method using micro-seismic monitoring and believed that the rock instability precursor can be captured by the response of micro-seismic information. Xue et al. (2021a) considered MS observing technology to detect real time responses of tunnel surrounding rock during its progressive failure, and stress/volume/frequency was captured for guiding on-site construction in real time and believed that this technique can solve the tricky faced. One can state that many researchers clarified basic precursors of ground collapse in high-stress rock bodies through the MS technology (Rigo et al. 1996; Wang et al. 2021; Yin et al. 2021; Zhao et al. 2021a). Several scholars have released plentiful reports covering early-warning/risk study of goafs using MS method. Nevertheless, there are few research reports on the MS monitoring results and laws of roof stability in shallow goaf subjected to several blasting disturbances which are important for evaluating whether the open pit mine can continue to work safely.

The current investigation releases the stability of the goaf occurred in an open pit mining and uses a three-dimensional (3D) laser detector to perform fine modeling of the goaf. MS observing technique is established for exploring progressive failure process of rock mass surrounding the goaf under blasting disturbance as a function of cumulative variations in various factors (e.g., apparent stress/volume). The features and signs linked with the failure of goafs could analyze in advance.

2 Background and goaf detection

The field work was undertaken in a Chinese open pit iron-rich ore mining site. After uneven mining and fast excavating operations, some goafs have been created in this mining zone. As a result of open pit expansion/extension, the goaf has posed a great threat to the normal mining production and brought great difficulties to both extraction/use of deep Fe-rich ores and mining plans' application. Underground goaf seriously threatens the security of huge mining tools, and leads to severe potential safety hazards to mine's security/basting feature. As shown in Fig. 1, on 15 April 2016, No. 13 drilling rig in E-4049.458 m, N-242.721 m and H-209.8 m in single tree expansion zone formed the hole with an east–west length of about 45m, a north–south length of about 44 m, an area of 1499 m^2 and a surface subsidence of 7 m. On 5 May 2016, a subsidence area was formed at E-3426.508 m, N-373.914 m and H-158.4 m of the single tree mining area, with an east–west length of about 3.2 m, a north–south length of about 2.9 m and an area of 8 m^2 and a surface subsidence of 0.1 m.

Figure 1 displays 3D laser scan technology being used for exploring the volume/shape of goafs by installing the MS monitoring system. Specific operation stages have been followed: In a potential goaf area on + 145 m platform, vertical holes are firstly drilled by a shallow hole-drill rig, penetrating goaf's roof. Goaf boreholes are then introduced in different directions. After these two important actions, 3D laser scan has been employed for receiving goaf scan models in varied ways, splicing goaf scan models as stated by the confirmed coordinate points. In conclusion, the shallow goaf's geometry/size has been determined eventually.

3 Establishing an in-situ MS monitoring system at the goaf

Micro-seismic refers to the vibration generated by seismic waves during the development of cracks in rocks within a limited zone caused by the induced factors (e.g., digging). MS observing technique is use of recording/analyzing MS wave information to obtain data on the time, source location, magnitude, energy release, and nonlinear strain area of micro-seismic activity in rock masses, to judge, assess, and predict rock mass stability within the range of observing. Before the failure of rock mass, accumulated energy is mostly unrestricted in elastic wave form (i.e. micro earthquakes). The energy's intensity causes variations

Fig. 1 Mining subsidence area caused by irregular mining and goaf detection process of studied mine site
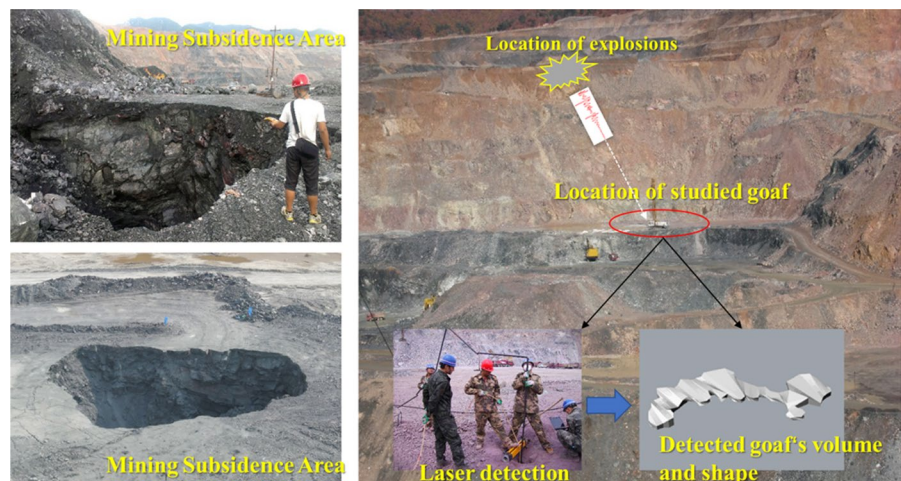
as instability may happen. So every elastic wave (MS wave) includes useful knowledge on the changes in rock mass's internal state. If several probes are settled in an assured array form nearby damaged area to create a probe range, and as micro-seismic appear in observing body, sensors can collect micro-seismic signs and alter it into voltage/charge. The period as each probe takes any sign is measured by multi-point synchronous data gathering, and directs of each probe and the gauged wave speed are substituted into equation set for solution, The spatio-temporal parameters of the micro-seismic source can be determined for positioning purposes. The schematic diagram of

micro-seismic monitoring principle is shown in the Fig. 2. The specific installation and testing process is described below.

(1)   Selection of sensors

According to the empirical data of mine micro-seismic monitoring, it can be concluded that there is an empirical relationship between the type, frequency and layout density of sensors of mine's MS observing method and the earthquake intensity and monitoring range (Table 1).

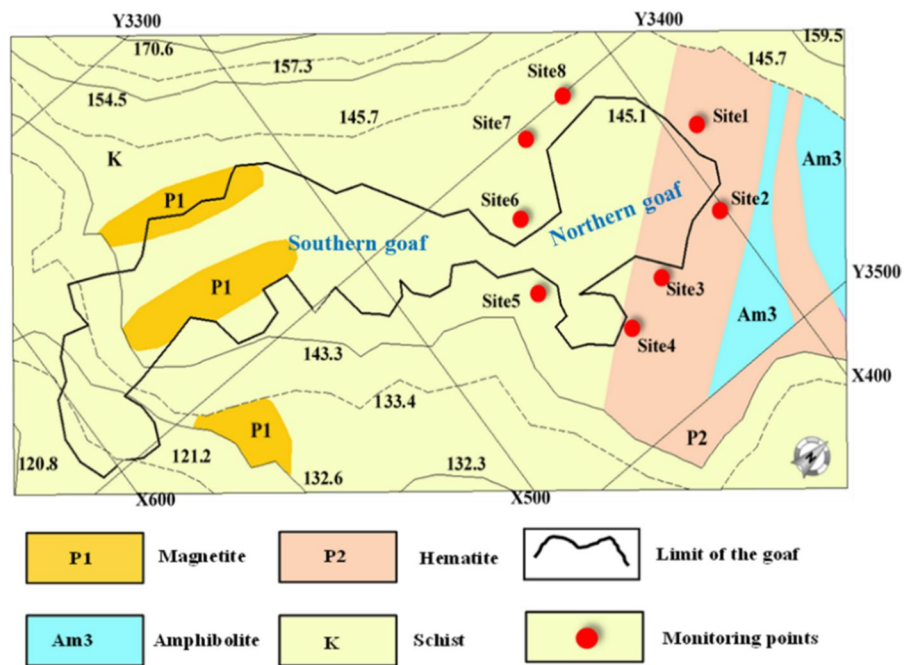**Fig. 2** Detailed arrangement scheme of the micro-seismic monitoring

Table 1 Relationship between sensing limits and the scope of monitoring area

Minimum magnitude	Maximum magnitude	Average volume (km³)	Number of events (day)	Sensor		Minimum density (km)	Bandwidths (Hz)
				Type	Frequency (Hz)		
1–0	4~5	30×30×5	100	Velocimeter	1; 4.5	Minimum five sensor spacing > 2	0.5–300
0–1	4	3×3×3	1000	Velocimeter	4.5; 28	Minimum five sensor spacing < 1	2–2000
−3 to −4	3	0.3×0.3×0.3	10,000	Accelerometer	10,000	Minimum five sensor spacing < 0.3	3–10,000

Table 2 Technical factors of 14 Hz-speed sensor

Parameters	Index
Frequency range (± 3 dB)	6–2000 Hz
Open circuit damping	$0.185 \pm 5\%$
Standard coil resistance	$3500\,\Omega \pm 5\%$
Open circuit sensitivity	80.0 V/m/s $\pm 5\%$
Damping (0.7) sensitivity	56.1 V/m/s $\pm 5\%$
Diameter	51 mm
Length	300 mm
Weight	1.3 kg
Installation hole diameter	More than 76 mm
Installation test water depth pressure	600 m

The surface elevation of the northern vacant area in the Xiaobeigou area is $+145.1$ m, about 65 m long and 48 m wide, and the average thickness of the roof is about 24 m. Considering the impact of blasting operation and geological structure on the upper bench, the monitoring range can reach at least a spatial scale of 200 m long, 150 m wide and 50 m high. Therefore, the velocimeter with a natural frequency of 14 Hz is selected as the micro-seismic sensor for the network construction in the Xiaobeigou vacant area for micro-seismic monitoring. Table 2 shows relevant technical factors.

(2) Micro-seismic sensor layout scheme

In view of shallow goaf's features, the 8-channel micro-seismic monitoring system established by IMS (Institute of Mine Seismology) having instantaneous performance and strong precision is selected as a monitoring means by comprehensive comparison and analysis from all aspects. System's hardware is alienated into three fragments: probes, and data collector/communication parts.

For Xiaobeigou goaf, roof's thickness in the south zone is 12–20 m, the roof scum's width is nearly 5 m, the actual roof thickness is only 7–15 m, and the roof thickness is thin; Roof's width in the north zone is between 22 and 26 m, the thickness of the roof scum is between 2 and 3 m, and the actual thickness of the roof is about 20 m. Considering the favorable principle of micro-seismic station layout, micro-seismic sensors are suitable for the north area. At the same time, in view of the limitation of the number of channels and sensors of MS observing method, it is arranged in northern area of the Xiaobeigou goaf. In order to avoid that the sensors are not in a straight line and a plane as much as possible, during the construction of sensor drilling, it is ensured that the drilling holes are not at the same elevation, and the inclination of the drilling holes are also different to ensure the monitoring accuracy of micro-seismic as much as possible. Figure 2 displays the selected sensor layout scheme while and Table 3 lists 3D spatial coordinates of the sensor.

(3) Positioning accuracy test

To obtain accurate spatial location of micro-seismic events, it is necessary to conduct blasting location test. According to the rock sample data sampled and tested on site, the propagation velocity of longitudinal wave is mostly between 2500 and 3700 m/s. Thus, the mean propagation speed of P and S waves in rock mass is initially set as 3000 and 1800 m/s, respectively, and velocities of P and S waves calibrated by blasting test are 2709 and 1564 m/s, respectively. For wave velocity correction, fixed-point blasting on site (with specific three-dimensional coordinates of the blasting point known) are used, pick up the blasting waveform through micro-seismic sensors, and then calculate the longitudinal and transverse wave velocities of the rock mass to complete wave velocity correction. The positioning error of blasting events obtained by using the above wave velocity is shown in the Table 4. Two blasting tests in the target research area were conducted and the blasting coordinate positions through a micro-seismic monitoring system were retrieved. The

Table 3 Probe's coordinate information

Sensor number	Coordinate		
	X	Y	Z
Site1	-461.039	3436.331	139.603
Site2	-459.993	3420.297	139.381
Site3	-445.035	3411.217	139.988
Site4	-430.224	3403.113	135.994
Site5	-392.948	3457.399	136.321
Site6	-410.720	3468.852	140.289
Site7	-437.033	3462.172	135.927
Site8	-454.774	3475.973	138.229

Table 4 Blasting events' locating outcomes

No	Blasting place (m)		Event zone (m)		Fault (m)
1	X	3607.94	X	3605	5
	Y	−192.1	Y	−197	
	Z	181.9	Z	184	
2	X	3557.548	X	3563	6
	Y	−164.9	Y	−161	
	Z	183.4	Z	179	

inversion results indicate that the errors between the calculated coordinates of the two blasting positions and the actual positions are 5 m and 6 m, respectively. Therefore, the positioning accuracy of MS observing method in project can meet the engineering requirements.

4 Results and discussions

4.1 Features of MS activity following blast mining

4.1.1 Development of magnitude and time

For the implementation of MS observing method in the goaf on December 3, 2018, the system has run smoothly except for a few brief signal losses caused by the failure of the MS monitoring equipment on February 22–March 4, March 21–31, and May 1–6, 2019. As of June 3, 2019, a total of 159 MS positioning events have been monitored, and the distribution of MS event activity over time is shown in Fig. 3. On January 2, 2019, a large-scale blasting action was performed on goaf's upper platform. Following the blasting disturbance, the MS activity rate increased, and six MS events occurred on January 4. In mid-April, a small-scale blasting action was executed over +192 m platform in goaf's upper part, and the MS activity rate increased again due to this blasting disturbance.

Figure 4 displays the magnitudes of MS cases. During monitoring period, the MS cases ranged from −2.5 to 1.2, and 24 MS events with magnitudes greater than 0 were concentrated between −2.5 and 0 (accounting for 84.91%), signifying that rock mass was mainly impaired by microcracks during monitoring. According to the statistics of events during the monitoring period, a distribution map is constructed to illustrate the MS events over 24 h. MS cases are intense between hours of 12:00–16:00 every day. This is because the blasting operations in the mine are conducted at approximately 12:00 every day; under special circumstances, blasting can be delayed until about 15:00 at the latest. Following a blasting disturbance, rock mass in the observing space is slightly fractured; the other time periods mainly correspond to the shovel transportation stage and cone drilling stage. There is no blasting/mining activity during these two stages, and as a result, there are relatively few MS cases. Occurrence of MS cases are consistent with blasting operations, which suggests that
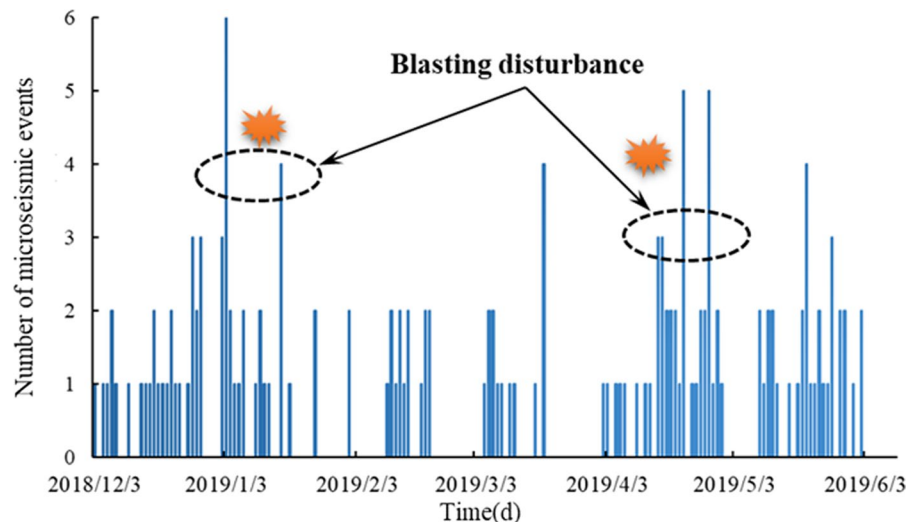

Fig. 3 Scattering of MS event activity

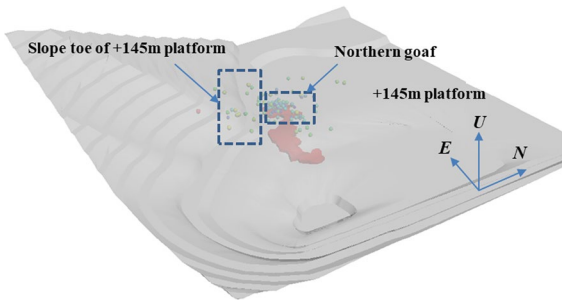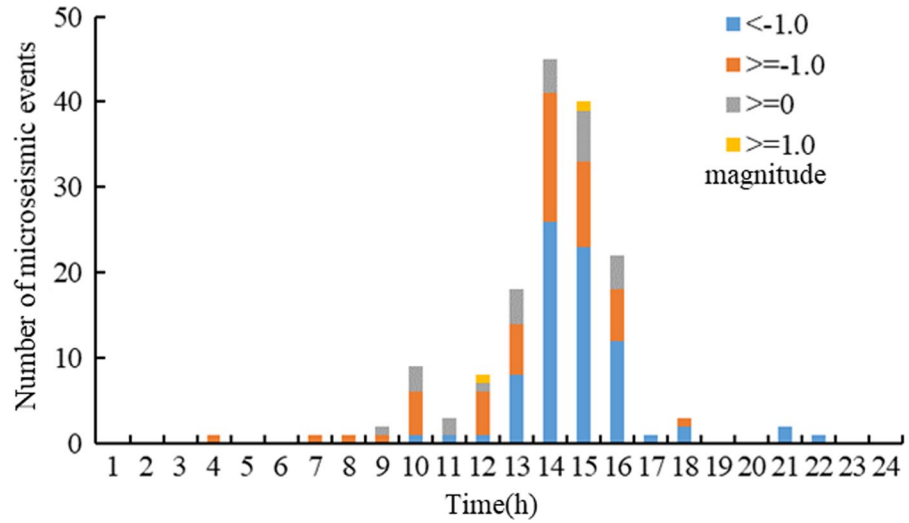**Fig. 4** Distribution of MS events over 24 h

Fig. 5 MS cases' spatial distribution

occurrence of MS cases is strictly linked with mining activities.

4.1.2 Evolution of MS cases over time

The spatial-distribution of MS cases from December 3, 2018, to June 2, 2019, is shown in Fig. 5. MS cases are intense in northern goaf and at foot of +145 m platform slope. Because there was no mining activity on +145 m platform during this time interval, it can be concluded that MS cases were triggered through the upper bench blasting disturbance and rock mass's creep itself.

It is clear from Fig. 6 that the number of MS cases during monitoring gradually increased from 28 (at the end of December 18, 2018) to 159, and the accumulation of events continuously migrated and expanded, moving to the upper roof of the goaf

and the outer area of the slope foot. Large-magnitude actions are mainly focused on overlying strata (zone A) at eastern boundary of the +145 m platform and at the foot of the upper platform slope. MS actions in zone A are mostly triggered by upper bench blasting disorders. By April 30, 2019, the number of MS cases in area A stopped increasing, thus forming a high-stress area with 3–4 m width. Owing to the slight number of MS cases, microcracks represent main defects in the area. As shown in Fig. 6b, by January 31, 2019, a vertical fracture A, an arched fracture B, and an arched fracture C were designed in the covering layer of the goaf. The arched fracture B's height was approximately 10.3 m, and the height of arched fracture C was approximately 3.2 m. These observations indicated that there were weak interlayer separation cracks in the overlying strata of the goaf, although there were no clear mining cracks. Additionally, there are a few MS events laterally clustered between fracture A and the foot of the slope. On February 28, 2019 (Fig. 6c), following the initiation and development of microcracks, the transverse and vertical cracks at fracture A penetrated, and the fracture zone at the foot of the upper platform slope initially formed in the northern goaf. Under the mechanical action of continuous creep of goaf's overlying strata, microcracks in mining-induced breakage field continued to breed and expand, and the influential range of arched cracks B and C moved to the upper part of the goaf. By June 2, 2019, the height of arched
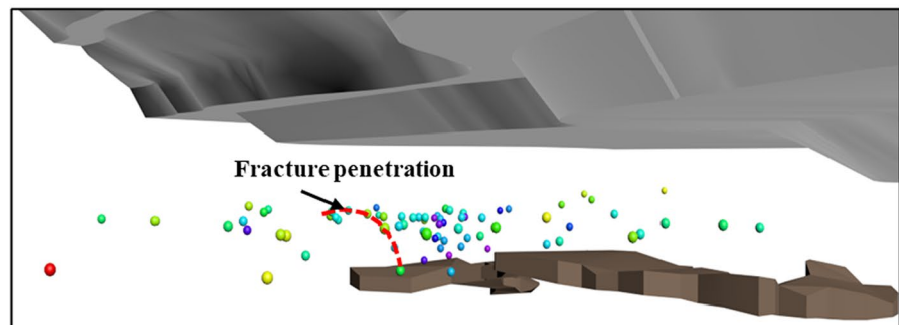
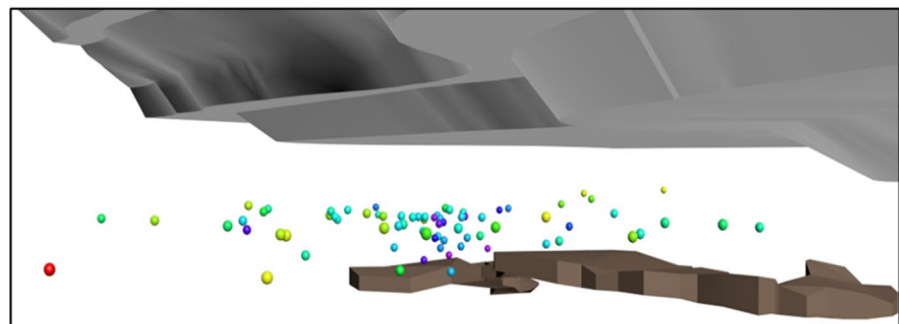**Fig. 6** Scattering of MS cases during monitoring
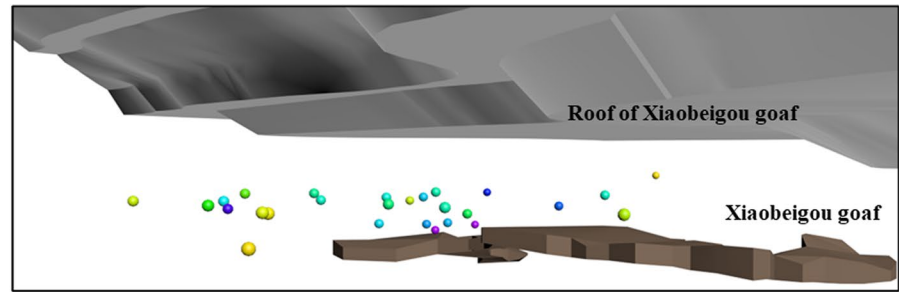
(a) MS event distributions up to December 23, 2018
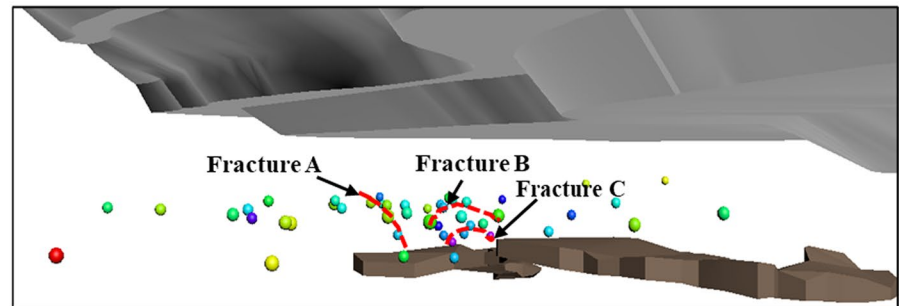
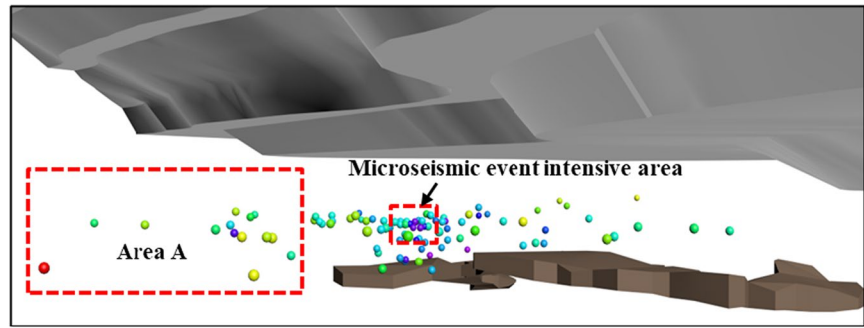(b) MS event distributions up to January 16, 2019
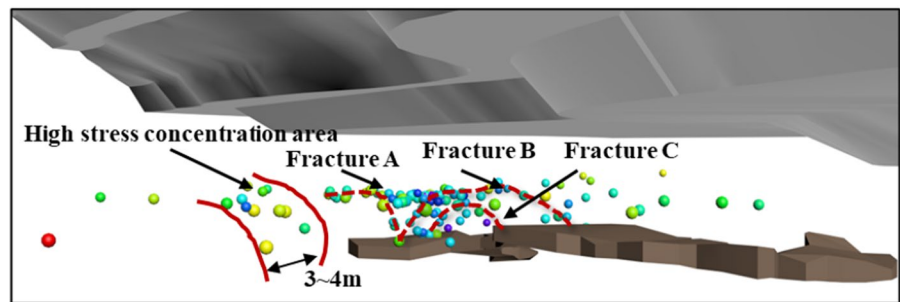
(c) MS event distributions up to February 21, 2019

(d) MS event distributions up to April 13, 2019

Fig. 6 (continued)

(e) MS event distributions up to April 30, 2019

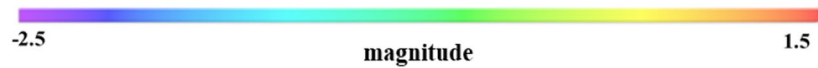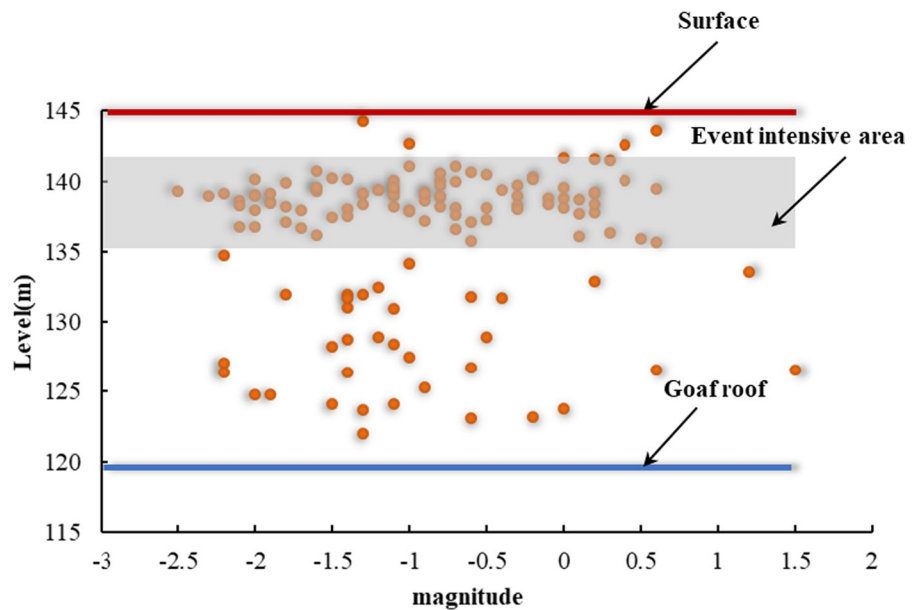(f) MS event distributions up to June 2, 2019

Fig. 7 Height distribution of MS cases

crack B was approximately 15.6 m (i.e., 5.3 m higher than the initial height), and its distance from the surface was approximately 4.4 m; the height of arch crack C was approximately 5.1 m (i.e., 1.9 m higher than the initial height). The left arch angle of the two arched fracture areas corresponds to the area of MS case accumulation (Fig. 6e), which is the most likely point to succumb to roof instability and failure in the goaf.

4.1.3 Distribution of MS event elevations

The link between MS case elevation and magnitude is shown in Fig. 7, where dots represent the locations of MS cases. MS cases are distributed throughout the overlying strata of the goaf roof owing to crack initiation in the roof strata caused by blasting disturbance. Cracks continue to develop until they penetrate under the action of creep deformation.

According to these location results, MS cases are distributed in the range of $+135$ to $+142$ m, within approximately 15–22 m from the goaf roof. The distribution of MS case elevation reveals no clear three-zone characteristics. The $+140$ m elevation where MS cases accumulate is only ~ 5 m in vertical distance from the ground surface. If the roof in the goaf is unstable and destroyed, it would very likely induce the sudden collapse of the ground surface. During the monitoring period, there were few MS cases without large-scale cracks, and 71.7% of MS positioning cases with magnitudes ≤ 0.5 occurred within the blasting disturbance influential range (i.e., $+135$ to $+140$ m).

4.2 Analysis of goaf deterioration based on changes in the source parameters

Numerical approaches are usually applied to explore MS cases in certain time/space domains to evaluate the laws with changes in time/space (Cheng et al. 2019; Liu et al. 2021; Xue et al. 2021b). Numerical factors include apparent volume/stress and average displacement, which are defined as follows:

Stress (σ_A) signifies home rock mass's stress step, which is demarcated to be MS energy emitted by rock mass in inflexible strain area of unit, as expressed in Eq. (1),

$$\sigma_A = \frac{E}{P} = \eta\overline{\sigma} \qquad (1)$$

where $\tilde{\sigma}$ is shear stress carrying out on fault, E is emission MS energy, P is potential change of microseismicity, and η is seismic efficiency.

Volume (V_A) signifies inelastic rock mass deformation's bulk, which is estimated based on recorded waveform factors. The slope of the accumulated volume changes over period may express rock mass's strain rate, as expressed in Eq. (2),

$$V_A = \frac{\mu P^2}{E} \qquad (2)$$

where μ is rock mass's shear modulus.

The mean dislocation on fault plane ($\overline{D}$) is another crucial factor for evaluating mine risks, and the distortion of source rock mass due to failure can be expressed by the displacement, as defined in Eq. (3),

$$\overline{D} = \frac{M_0}{\mu\pi r_0^2} \qquad (3)$$

where M_0 is the MS instant, and r_0 is the fault plane's radius.

In this section, the information and law of deterioration process of goaf will be obtained through the evolution process of source parameters with time.

4.2.1 Time domain scattering of cumulative volume, stress and displacement

Figure 8 shows entire time domain deviation of apparent stress, cumulative apparent volume, and cumulative displacement for each MS case during MS monitoring. From the experimental results, some outcomes could be interpreted below:

(1) Mean apparent stress in region I exhibits limited changes. The maximum value (0.03 MPa) corresponds to elastic step, and energy in rock mass accumulates endlessly. Between December 3–17, 2018, the cumulative displacement increased slowly, and the rock cracks expanded steadily, without a large degree of penetration. This period represents the gestation stage of rock mass failure.

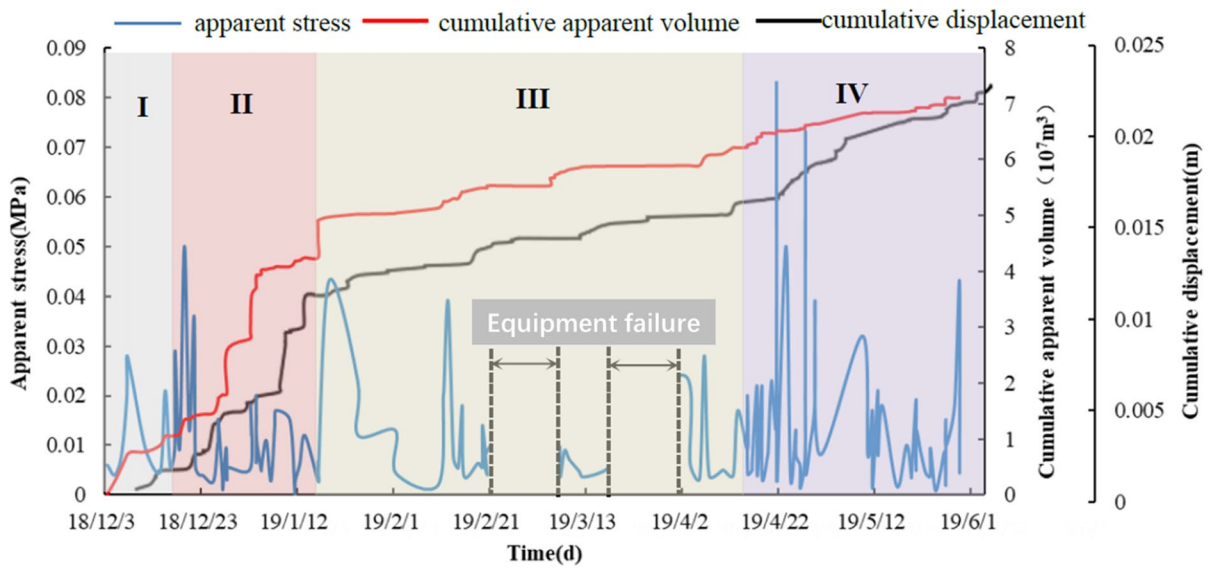(2) On December 18, 2018, the stress in region II swiftly increased to 0.05 MPa. Stress's average

Fig. 8 Variations in the cum. apparent vol., cumulative displacement, and stress

level increased from December 23rd, when rock mass had grasped yield state; this shows crack penetration and impending large-scale rock mass failure. On December 24th, stress suddenly fell a low level, and energy stowed in rock mass was unrestricted. Simultaneously, cumulative displacement slope increased, the crack propagation rate accelerated, the cumulative volume increased significantly in a step-wise fashion, and rigid distortion volume of rock mass augmented. The rock mass cracked (Fig. 6b), thus forming three main cracks defining the crack propagation stage of rock mass.

(3) From January 14 to February 21, 2019, the apparent stress in region III experienced several "sudden rises-sudden drops"; the capacity of the rock mass enables many "incubation-release" events. The cumulative displacement exhibited three sudden jumps on January 14th, January 24th, and February 4th, and the slope was almost zero from February 4–12. This specified that rock mass was damaged between January 14th and February 4th, allowing the main crack to penetrate further, as shown in Fig. 6c. These events comprised the crack penetration stage. The period from February 18 to April 13 was a quiet period, during

which there were very few MS cases, and most of the events involved the initiation and development of new microcracks.

(4) The stress in region IV increased suddenly again after the quiet period, reaching 0.083 MPa. On April 14th, 2019, the cumulative displacement slope began to increase, and fractures developed rapidly in rock mass. Meanwhile, the cumulative apparent volume underwent many sudden increases, and the nonlinear distortion of rock mass increased continuously. Many micro-earthquakes occurred during this period (Fig. 6e). On May 11th, the apparent stress dropped sharply and again reached a low-stress level, thus entering the second quiet period.

The cumulative apparent volume increased stepwise in the first three stages; in the last stage (after April 14, 2019), it mostly involved mutation and rising, which indicates that there were distinct rock mass deformation modes before versus after April 14. Figure 6e shows that the new micro-seismic event accumulation area after April 14 is the arch shoulders of arched cracks A and B. According to the moment tensor analysis formula of rock mass fracture, this area was determined to comprise mixed tension and shear
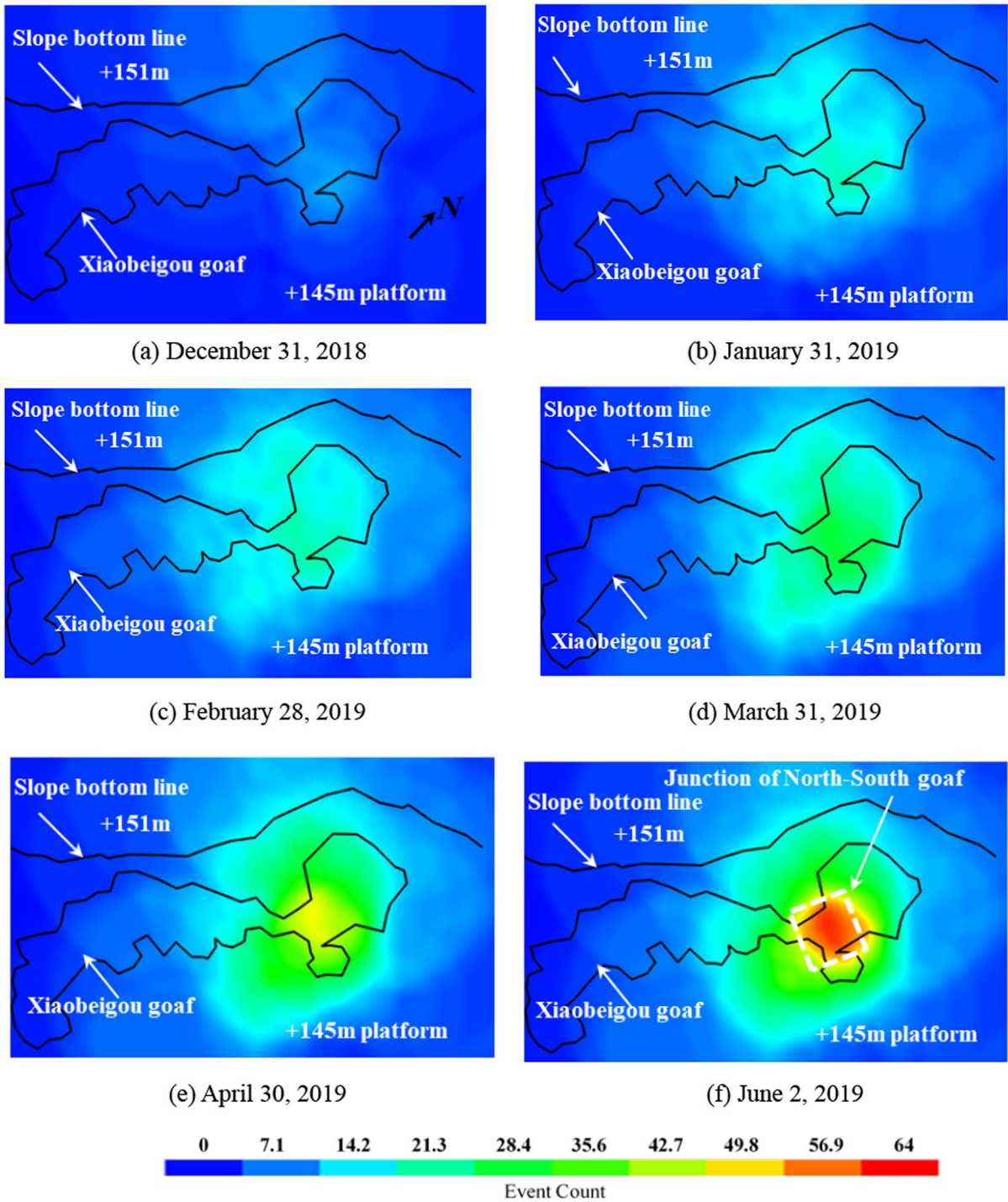
Fig. 9 MS events' dynamic density distribution

failure mechanisms, and the main failure before April 14th was tensile failure. During monitoring, max. apparent stress was 0.083 MPa, and stress level was generally low. The entire process remains in the cycle of microcrack "initiation-development-penetration". Currently, the goaf is in a fairly steady form based on site investigations, and MS monitoring results provide technical support for subsequent blasting to avoid hidden dangers in the goaf.

4.2.2 Spatial scattering of event density, stress and displacement

Figure 9 shows the plane projection of dynamic density scattering of MS cases. At early monitoring, MS cases were mainly distributed in the northern goaf and slope bottom line (Fig. 9a). By the end of January 2019, MS cases were distributed in border area between north and south goaf areas. By February 28th, the distribution range of events in the northern
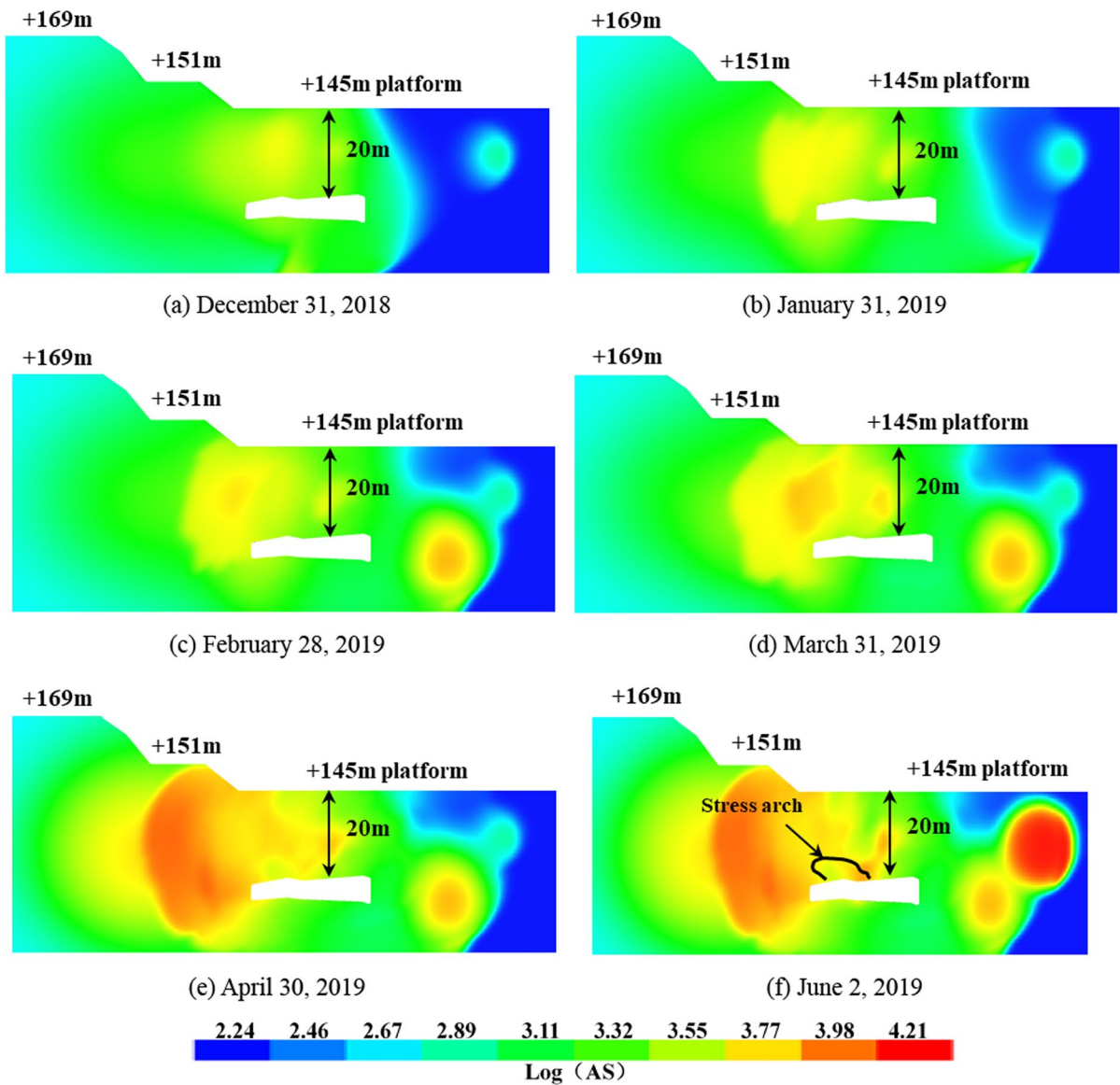

(a) December 31, 2018

(b) January 31, 2019

(c) February 28, 2019

(d) March 31, 2019

(e) April 30, 2019

(f) June 2, 2019

Fig. 10 Apparent stress evolution process

goaf was further expanded, and event number in area by the northern goaf to slope's bottom line increased. By March, the distribution of events covered the entire northern goaf. By the end of April (following the upper bench blasting disturbance), the distribution range of events at the bottom line of the slope expanded to the southern goaf, and the number of events at the junction of the north and south goafs increased sharply, revealing clear agglomeration phenomena. By June 2nd, there were 64 events at the junction between the north and south empty areas. Geological data from around the mine indicate that it is at the interface between ore body and rock layer. The plane projection of the dynamic density distribution map of events reveals that the interfacial area between north and south goafs is a dangerous area, which requires special attention during production operation and goaf blasting.

The stress's analysis was carried out, as shown in Fig. 10, according to the XII exploration line in Fig. 2. During rock mass failure's incubation time, the apparent stress was mainly concentrated in the goaf roof (Fig. 10a) because of the deterioration of the goaf roof before the monitoring system was deployed. Moreover, the roof's stress increased constantly under goaf side's stress and nearby rock's gravity. The cracks expanded continuously from bench side to goaf's left side due to the blasting disturbance of the upper bench, and the stress range also expanded continuously (Fig. 10b). It is clear from Fig. 8 that there were several "sudden rises-sudden falls" in terms of stress in February 2019. Energy in rock mass was inoculated and unrestricted many times, which allowed the initiated cracks to penetrate further and form a stress concentration area at the 45° side angle joint between the side part and the left part of the goaf. Meanwhile, following the blasting disturbance of the +128 m platform, a high-energy microseismic event occurred at the side foot of the +145m platform, thus inducing a small-scale stress concentration phenomenon (Fig. 6c). As the fracture further expanded to free surface of goaf, stress concentration ranges also shifted to goaf's left and corner sides, while degree of deterioration increased. On April 20th, the apparent stress reached a new peak and entered the yield state. A major quantity of energy that had gathered in rock mass was released rapidly within a few days, and stress focused at left side, 45° side angle, and roof, thereby forming a stress arch at

the left part of the goaf roof (Fig. 10f). The influential range of stress concentration was 17 m above the goaf roof and 8 m far from surface, and stress was small. Thus, it was determined that the goaf was relatively stable, and the stress arch at the left part of the goaf roof represents the point with the greatest potential for roof collapse failure.

Figure 11 shows displacement analysis carried out in the XII exploration line. During the energy incubation period, the deformation was mainly concentrated in the goaf roof's covering layer. Reason behind this is the same as that revealed by the stress nephogram, i.e., the goaf roof deteriorated before the end of the observing period, and cracks lasted to initiate and develop under the action of gravity. In the crack propagation stage (stage B), the deformation area extended from roof to goaf's left side corner, and rock mass at roof/side corner of the goaf exhibited major deformation (Fig. 11b). After many energy inoculation and release cycles (Fig. 8) in stage C, the deformation area expanded further, the degree of nonlinear rock mass deformation intensified, leaving the roof damaged (Fig. 11d).

Following the bench blasting disturbance in the goaf's upper part, the deformation area expanded further to the lower part of the +151 m platform side, the degree of crack penetration increased, the deformation area expansion accelerated, and goaf roof further worsened, thus forming a deformation concentration area (Fig. 11e). Before May 16th, rock mass was demolished, and most of energy was unrestricted. Thus, the degree of deformation decreased during the monitoring period starting from June 2nd, which resulted in little change to the overall deformation influential range; however, the deformation concentration area further expanded to the roof and sides. The deformation influential range of overlying strata in goaf is 4 m far from surface, and the deformation is small. Presently, the goaf is in a fairly steady form, considering the stress nephogram.

5 Conclusions

The instability/failure mechanism was investigated in this investigation in order to deliver a risk appraisal for a Chinese open pit goaf subjected to blasting disturbance. As a function of high-precision MS observing, goaf's nearby rock considering
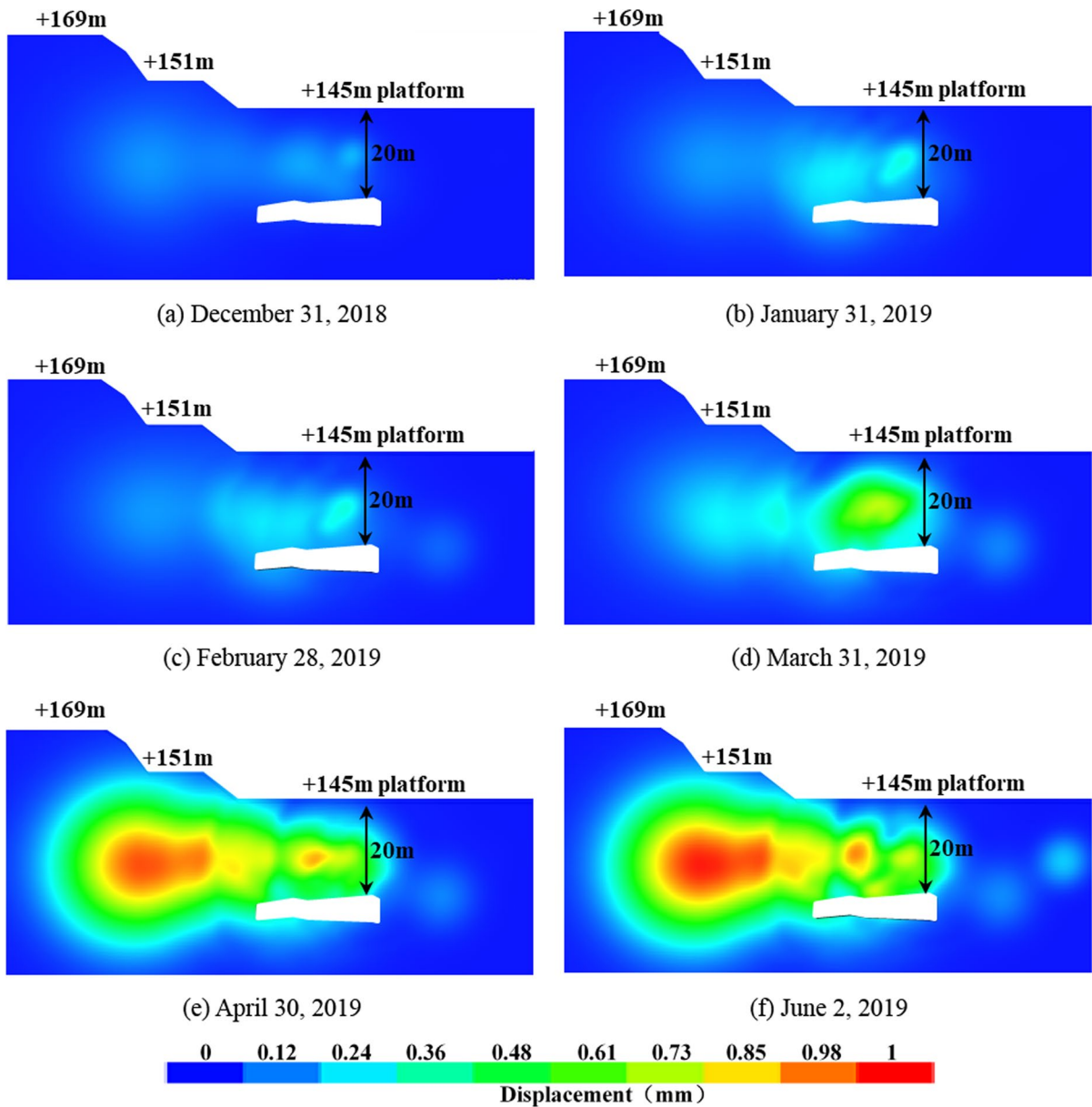
(a) December 31, 2018

(b) January 31, 2019

(c) February 28, 2019

(d) March 31, 2019

(e) April 30, 2019

(f) June 2, 2019

Fig. 11 Evolution process of the displacement

blasting disturbance was analyzed in terms of its failure behavior. The main deductions are below:

- Progress of MS cases indicated that goaf's roof had deteriorated before MS monitoring system was implemented. Following a blasting disturbance of the +169 m bench, two arched fracture zones with heights of 15.6 and 5.1 m were formed in the goaf roof, and an arc crack was shaped from goaf's roof to foot of +151 m step slope. MS cases mainly accumulated at +140 m in the vertical direction, with a vertical distance of only ∼5 m from the surface.

- MS cases accumulated at the rock-intersecting interface of the north–south goafs in the horizontal direction. If the goaf roof is unstable and damaged in the future, it is likely that the surface will suddenly collapse at the rock-intersecting interface. The evolution of source parameters shows that the goaf is currently in a stable state.

- Following three blasting disturbances, the left side corner's strain band and roof's tensile strain band were focused, and many micro cracks entered to generate cracks in terms of macro-scale.

Availability of data and materials The data/model/code backing this study's findings are accessible upon rational demand.

Declarations

Ethics approval and consent to participate Not applicable.

Consent for publication All authors approve this paper's publication.

Competing interests The writers state that they have no recognized challenging commercial benefits or private links that may seem to effect the study described in the present investigation.

References

Chen B, Shen B, Zhang S, Li Y, Jiang H (2022) 3D morphology and formation mechanism of fractures developed by true triaxial stress. Int J Min Sci Technol 32:1273–1284

Chen B, Shen B, Jiang H (2023) Shear behavior of intact granite under thermo-mechanical coupling and three-dimensional morphology of shear-formed fractures. J Rock Mech Geotech Eng 15:523–537

Cheng G, Li L, Zhu W, Yang T, Tang C, Zheng Y, Wang Y (2019) Microseismic investigation of mining-induced brittle fault activation in a Chinese coal mine. Int J Rock Mech Min Sci 123:104096

Dong L, Wesseloo J, Potvin Y, Li X (2015) Discrimination of mine seismic events and blasts using the fisher classifier, Naive Bayesian classifier and logistic regression. Rock Mech Rock Eng 49:183–211

Dyskin AV, Basarir H, Doherty J, Elchalakani M, Joldes GR, Karrech A, Lehane B, Miller K, Pasternak E, Shufrin I (2018) Computational monitoring in real time: review of methods and applications. Geomech Geophys Geo-Energy Geo-Resour 4:235–271

Emmanuel A, Jerry C, Dzigbodi D (2018) Review of environmental and health impacts of mining in Ghana. J Health Pollut 12:43–52

Ge M (2005) Efficient mine microseismic monitoring. Int J Coal Geol 64:44–56

Huang L, Li J, Hao H, Li X (2018) Micro-seismic event detection and location in underground mines by using convolutional neural networks (CNN) and deep learning. Tunn Undergr Space Technol 81:265–276

Huo X, Shi X, Qiu X, Zhou J, Gou Y, Yu Z, Zhang S (2022) A study on raise blasting and blast-induced vibrations in highly stressed rock masses. Tunn Undergr Space Technol 123:104407

Jia H, Yan B, Yilmaz E (2021) A large goaf group treatment by means of mine backfill technology. Adv Civ Eng 2021:3737145

Jia H, Yan B, Guan K, Liu H, Wu Q, Yin Y, Liu H (2022) Stability analysis of shallow goaf based on field monitoring and numerical simulation: a case study at an open-pit iron mine. China Front Earth Sci 10:897779

Juang CH, Gong W, Wasowski J (2022) Trending topics of significance in engineering geology. Eng Geol 296:106460

Karian T, Shimada H, Sasaoka T, Wahyudi S, Qian D, Sulistianto B (2016) Countermeasure method for stope instability in crown pillar area of cut and fill underground mine. Int J Geosci 07:280–300

Kaya A, Tarakçi ÜC (2021) Stability investigation of a deep shaft using different methods. Int J Geomech 21:05020009

Liu C, Li S, Cheng C, Cheng X (2017) Identification methods for anomalous stress region in coal roadways based on microseismic information and numerical simulation. Int J Min Sci Technol 27:525–530

Liu H, Zhao Y, Zhang P, Liu F, Yang T (2021) Stope structure evaluation based on the damage model driven by microseismic data and Mathews stability diagram method in Xiadian Gold Mine. Geomat Nat Haz Risk 12:1616–1637

Liu N, Pei J, Cao C, Liu X, Huang Y, Mei G (2022) Geological investigation and treatment measures against water inrush

hazard in karst tunnels: a case study in Guiyang, southwest China. Tunn Undergr Space Technol 124:104491

Ma K, Wang H, Liao Z, Peng Y, Wang K (2022) Precursor of microseismic energy and stress evolution induced by rockburst in coal mining: a case study from Xiashijie, Shannxi, China. Geomech Geophys Geo-Energy Geo-Resour 8:134

Mánica MA, Ciantia MO, Gens A (2020) On the stability of underground caves in calcareous rocks due to long-term weathering. Rock Mech Rock Eng 53:3885–3901

Maxwell SC, Rutledge J, Jones R, Fehler M (2010) Petroleum reservoir characterization using downhole microseismic monitoring. Geophysics 75:75A129-175A137

Ram S, Singh R, Kumar A, Singh AK, Kumar R, Rao AR, Rao VS (2022) Stability assessment of heightened rib/snook during extraction of a thick coal seam by continuous miner in single lift. Geomech Geophys Geo-Energy Geo-Resour 8:74

Rigo A, Lyon-Caen H, Armijo R, Deschamps A, Hatzfeld D, Makropoulos K, Papadimitriou P, Kassaras I (1996) A microseismic study in the western part of the Gulf of Corinth (Greece): implications for large-scale normal faulting mechanisms. Geophys J Int 126:663–688

Saeidi A, Heidarzadeh S, Lalancette S, Rouleau A (2021) The effects of in situ stress uncertainties on the assessment of open stope stability: case study at the Niobec Mine, Quebec (Canada). Geomech Energy Environ 25:100194

Seymour JB, Martin LA, Raffaldi MJ, Warren SN, Sandbak LA (2019) Long-term stability of a 13.7 × 30.5-m (45 × 100-ft) undercut span beneath cemented rockfill at the turquoise ridge mine, Nevada. Rock Mech Rock Eng 52:4907–4923

Talibe Keita AM, Jahanbakhshzadeh A, Li L (2021) Numerical analysis of the stability of arched sill mats made of cemented backfill. Int J Rock Mech Min Sci 140:104667

Tang CA, Wang J, Zhang J (2010) Preliminary engineering application of microseismic monitoring technique to rockburst prediction in tunneling of Jinping II project. J Rock Mech Geotech Eng 2:193–208

Tian X, Song Z, Zhang Y (2021) Monitoring and reinforcement of landslide induced by tunnel excavation: a case study from Xiamaixi tunnel. Tunn Undergr Space Technol 110:103796

Wang Y, Huang M, Wu A, Yao G, Hu K (2013) Rock backfill and hazard control of a bandoned stopes: a case study. Appl Mech Mater 368–370:1726–1731

Wang Y, Tang CA, Tang L, Zhang S, Li L, Li Y, Duan W (2021) Microseismicity characteristics before and after a rockburst and mechanisms of intermittent rockbursts in a water diversion tunnel. Rock Mech Rock Eng 55:341–361

Wang X, Liu Z, Gao X, Li P, Dong B (2023) Dynamic characteristics and energy evolution of granite subjected to coupled static–cyclic impact loading. Geomech Geophys Geo-Energy Geo-Resour 9:62

Xia K, Chen C, Zhou Y, Liu X, Zheng Y, Pan Y (2019) Catastrophe instability mechanism of the pillar-roof system in gypsum mines due to the influence of relative humidity. Int J Geomech 19:06019004

Xie H, Lu J, Li C, Li M, Gao M (2022a) Experimental study on the mechanical and failure behaviors of deep rock subjected to true triaxial stress: a review. Int J Min Sci Technol 32:915–950

Xie H, Zhang K, Zhou C, Wang J, Peng Q, Guo J, Zhu J (2022b) Dynamic response of rock mass subjected to blasting disturbance during tunnel shaft excavation: a field study. Geomech Geophys Geo-Energy Geo-Resour 8:52

Xu N, Li T, Dai F, Li B, Zhu Y, Yang D (2015) Microseismic monitoring and stability evaluation for the large scale underground caverns at the Houziyan hydropower station in Southwest China. Eng Geol 188:48–67

Xu L, Li Q, Mathias SA, Tan Y, Yang D, Fan C (2021) Strain characteristics and permeability evolution of faults under stress disturbance monitoring by fibre bragg grating sensing and pressure pulses. Geomech Geophys Geo-Energy Geo-Resour 7:93

Xue R, Liang Z, Xu N (2021a) Rockburst prediction and analysis of activity characteristics within surrounding rock based on microseismic monitoring and numerical simulation. Int J Rock Mech Min Sci 142:104750

Xue R, Liang Z, Xu N (2021b) Rockburst prediction and analysis of activity characteristics within surrounding rock based on microseismic monitoring and numerical simulation. Int J Rock Mech Min Sci 142:104750

Yan B, Jia H, Yilmaz E, Lai X, Shan P, Hou C (2022) Numerical study on microscale and macroscale strength behaviors of hardening cemented paste backfill. Constr Build Mater 321:126327

Yan B, Jia H, Yang Z, Yilmaz E, Liu H (2023) Goaf instability in an open pit iron mine triggered by dynamics disturbance: a large-scale similar simulation. Int J Min Reclam Environ 37:606–629

Yin S, Shao Y, Wu A, Wang H, Liu X, Wang Y (2020) A systematic review of paste technology in metal mines for cleaner production in China. J Clean Prod 247:119590

Yin X, Liu Q, Huang X, Pan Y (2021) Real-time prediction of rockburst intensity using an integrated CNN-Adam-BO algorithm based on microseismic data and its engineering application. Tunn Undergr Space Technol 117:104133

Zhang C, Tu S, Zhao Y (2019) Compaction characteristics of the caving zone in a longwall goaf: a review. Environ Earth Sci 78:27

Zhang Y, Liu Y, Lai X, Cao S, Yang Y, Yan B, Bai L, Tong L, He W (2023) Transport mechanism and control technology of heavy metal ions in gangue backfill materials in short-wall block backfill mining. Sci Total Environ 895:165139

Zhao Z, Sun W, Chen S, Feng Y, Wang W (2020) Displacement of surrounding rock in a deep circular hole considering double moduli and strength-stiffness degradation. Appl Math 41:1847–1860

Zhao J-S, Chen B-R, Jiang Q, Lu J-F, Hao X-J, Pei S-F, Wang F (2021a) Microseismic monitoring of rock mass fracture response to blasting excavation of large underground caverns under high geostress. Rock Mech Rock Eng 55:733–750

Zhao Z, Sun W, Chen S, Yin D, Chen B (2021b) Determination of critical criterion of tensile-shear failure in Brazilian disc based on theoretical analysis and meso-macro numerical simulation. Comput Geotech 134:104096

Zhou Z, Zhao Y, Cao W, Chen L, Zhou J (2018) Dynamic response of pillar workings induced by sudden pillar recovery. Rock Mech Rock Eng 51:3075–3090

Zhu W, Yan B, Liu X, Yang Z, Guan K (2022) Rock creep deformation triggered by dynamic disturbance: numerical simulation. Int J Geomech 22:04022101

Zhuang P-Z, Yang H, Yue H-Y, Fuentes R, Yu H-S (2022) Plasticity solutions for ground deformation prediction of shallow tunnels in undrained clay. Tunn Undergr Space Technol 120:104277

Zou Y, Ma G, Mei J, Zhao J, Zhou W (2021) Microscopic origin of shape-dependent shear strength of granular materials: a granular dynamics perspective. Acta Geotech 17:2697–2710